Journal of Electronic Materials (2022) 51:4824–4835
https://doi.org/10.1007/s11664-022-09747-9

ORIGINAL RESEARCH ARTICLE

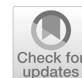

The Interfacial Properties of Monolayer MX–Metal Contacts

Ying Guo[1,2] · Gaoyang Zhao[1] · Feng Pan[2] · Ruge Quhe[3] · Jing Lu[4,5,6]

Received: 25 January 2022 / Accepted: 1 June 2022 / Published online: 22 June 2022
© The Minerals, Metals & Materials Society 2022

Abstract

Binary IV–VI chalcogenides MXs (SnS, SnSe, SnTe, GeS, GeSe, and GeTe), as a family two-dimensional (2D) semiconductor material, have a proper bandgap, high carrier mobility, stability in ambient conditions, and a pucker structure, hence they are potential channel materials for the next-generation electronic and optoelectronic devices. 2D MXs devices should directly contact the metal electrodes to inject suitable types of carriers, on account of the random dopant fluctuation. However, a Schottky contact is always formed at the interface, which degrades the performance of the MXs devices. Herein, we report the contact characteristics of the MXs field-effect transistors (FETs) with Graphene(Gr)/Ag/Au electrodes (two-interface model) by using quantum transport calculations and density functional theory. At the vertical interface, the MXs FETs form Van der Waals (vdW) contact type after being contacted with the Gr electrode, and an Ohmic contact is formed after being contacted with Ag and Au electrodes. At the lateral interface, the SnTe (armchair and zigzag), GeS (zigzag), and GeSe (zigzag) FETs with Gr electrode get a desired *p*-type Ohmic contact or quasi *p*-type Ohmic contact, suggestive of high device performance in such an MXs device. Our simulation provides a theoretical foundation for the choice of suitable electrodes in future ML MXs devices.

Keywords Density functional theory · quantum transport simulation · schottky barriers · monolayer MXs

Introduction

Recently, the size of silicon transistors shrank into the sub-10 nm, and Moore's law is still encountering technical bottlenecks due to short-channel effects. Two-dimensional (2D) semiconductor materials, such as transition-metal dichalcogenides and group-V-enes, are considering an alternative to silicon for the next decade because they have unique characteristics of electronic and optical properties. Although bulk channel materials can be manufactured to be very thin, 2D semiconductors have unique advantages. Thanks to their atomic-scale thickness and clean surface, the 2D semiconductors have better gate electrostatics and carrier transports than their bulk counterparts.[1] Consequently, 2D sub-5 nm transistors, such as MoS_2 field-effect transistors (FETs) with 1 nm gate length or 4 nm channel length, have been synthesized. Meanwhile, MoS_2 and black phosphorus (BP), the most researched 2D semiconductor, have low carrier mobility and poor air stability.[2,3] Therefore, it is very imperative to search for a kind of 2D semiconductor in the next electronic device generation.

As another 2D semiconductor family material, binary IV–VI chalcogenides MXs (SnS, SnSe, SnTe, GeS, GeSe,

✉ Ying Guo
guosophia@163.com

✉ Gaoyang Zhao
zhaogy@xaut.edu.cn

✉ Jing Lu
jinglu@pku.edu.cn

1 School of Materials Science and Engineering, Xi'an University of Technology, Xi'an 710048, People's Republic of China

2 School of Physics and Telecommunication Engineering, Shaanxi Key Laboratory of Catalysis, Shaanxi University of Technology, Hanzhong 723001, People's Republic of China

3 State Key Laboratory of Information Photonics and Optical Communications and School of Science, Beijing University of Posts and Telecommunications, Beijing 100876, People's Republic of China

4 State Key Laboratory of Mesoscopic Physics and Department of Physics, Peking University, Beijing 100871, People's Republic of China

5 Collaborative Innovation Center of Quantum Matter, Beijing 100871, People's Republic of China

6 Peking University Yangtze Delta Institute of Optoelectronics, Beijing 100871, People's Republic of China

and GeTe) have a proper bandgap (0.86–1.79 eV) that coincides with the range of visible light.[4,5] Similar to more recently studied BP, ML MXs have pucker structures, issuing in an in-plane anisotropic mechanical, electrical, and optical properties.[6–8] Compared with isotropic materials, an anisotropic material has an effective mass anisotropy, such as ML BP has a small effective mass (along the armchair direction) and a large effective mass (along the zigzag direction). This results in a large density of states in the transport direction and a superiority as the channel of devices.[9,10] Moreover, MXs are composed of low-toxic and earth-abundant elements and are stable in ambient conditions, and have high carrier mobility (on the order of the magnitude of 10^3 cm^2 V^{-1} s^{-1}).[11] Therefore, it is quite promising for ML MXs to be used in electronics and optoelectronics applications.[12] According to *ab initio* quantum transport simulations, ML GeSe, GeS metal-oxide-semiconductor field-effect transistors (MOSFETs) and ML GeSe, SnSe tunneling field-effect transistors (TFETs)[13–15] can satisfy the high-performance (HP) applications of the International Technology Roadmap for Semiconductors (ITRS).

However, in real 2D semiconductor transistors, such as 2D electronic and photoelectronic devices, the channel will contact metal electrodes so as to inject suitable types of carriers. A Schottky contact (Schottky barrier) always formed at the interface of 2D semiconductors and electrodes due to the metal-induced gap states (MIGS) and gap states, decreasing the carriers' transport and photoresponse efficiency, thus degrading the performance of 2D semiconductor devices.[16] Low Schottky barrier is crucial in obtaining a high on-state current in logic transistors as well as in having large photoresponsivity in photoconductors. It is a very significant problem for 2D transistors to remove or reduce the contact barrier and then improve the performance of the device. The classical doping method is not suitable for 2D semiconductor transistors due to the random dopant fluctuation. Therefore, selecting a suitable electrode with an Ohmic contact or quasi Ohmic contact (with a small Schottky barrier height (SBH)) at the interface is very important. The corresponding transistor is called the Schottky barrier FETs, the performance of which is often lower than that of MOSFETs. Hence, it can be seen that the interfacial properties of 2D transistors are concerned with their applications. Specific interfacial properties of some 2D FETs have been investigated in various theoretical kinds of literature, such as interfacial properties of ML GeSe with Cu, Ag, Ti, Au, Pd, Pt, Graphene(Gr), and Gr-Cu electrodes have been simulated, and Gr, Gr-Cu electrode formed a quasi Ohmic contact.[17] ML SnS with Ag, Al, Au, Pd, Cu, and Ni electrodes are also simulated.[18] However, since ML MXs have significant anisotropic properties, there is still a lack of systematic comparative study of the performance of MXs in contact with metal electrodes along with armchair and zigzag directions, and the prediction of interfacial properties is very helpful in developing 2D MXs transistors.

Herein, by using *ab initio* quantum transport simulation (QTS) and the density functional theory (DFT), we report studies on the performance of ML MXs FETs with Gr, Ag, and Au electrodes. We find that the band structure of ML MXs is preserved very well when put in contact with the Gr electrode, and the compound systems have weak bonding energy and a Van der Waals (vdW) binding type in the vertical interface due to having a larger interfacial distance and minimum atom-to-atom distance (> 3 Å). Meanwhile, MXs FETs with Ag/Au electrodes have strong bonding energy and an Ohmic contact because ML MXs undergo metallization at the vertical interface. In the lateral interface, the MXs FETs with Gr electrode have a *p*-type Schottky contact with hole SBH of 0.05/0.1 (GeSe zigzag/armchair), 0.08/0.29 (GeS zigzag/armchair), 0.09 (SnTe zigzag), 0.27/0.63 (GeTe zigzag/armchair), and 0.54 (SnSe zigzag) eV, respectively, and an *n*-type Schottky contact with electron SBH of 0.59/0.81 (SnSe armchair/zigzag) and 0.6 eV (SnSe armchair), respectively. Intriguingly, a desired Ohmic contact (*p*-type) is identified in the lateral interface of SnTe (armchair), and GeS-, GeSe-, and SnTe-Gr FETs along the zigzag direction which can be seen as a quasi *p*-type Ohmic contact for a small SBH. Either Ohmic contact or quasi Ohmic contact is very well beneficial for MXs device applications.

Computational Method

Figure 1 shows the (a) top view, (b) side view in the zigzag direction, and (c) side view in the armchair direction of pucker ML MXs. The structure anisotropy factor κ (defined as $\kappa=(a-b)/(a+b)$) and lattice parameters of optimized ML MXs (GeS($a=4.47$, $b=3.67$), GeSe($a=4.26$, $b=3.98$), GeTe($a=4.38$, $b=4.24$), SnS($a=4.44$, $b=4.03$), SnSe($a=4.52$, $b=4.26$), and SnTe($a=4.64$, $b=4.56$)) are shown in Table I, and they are in agreement with the formerly literature.[5,6,19–24] Three metal electrodes (Ag, Au, and Gr) are considered for their suitable work functions (4.26 eV, 5.10 eV, and 4.60 eV) because Ag and Au substrates are always used for MXs devices in experimentation,[8,23–27] and Gr electrode always improve the performance of devices.[28–33]

In the previous simulation works, 4–6 metal atomic layer is always used in the 2D material contacted metal electrodes, and the results show agreement with the experiments.[34] ML MXs and metal electrodes have a mutual effect only in several top layer metal atoms, in the preceding convergence tests, a six-layer metal model is made to meet the electrode requested of devices and fixes the bottom atomic positions to simulate the bulk metal electrode.[33,34] To avoid pseudo interaction in the

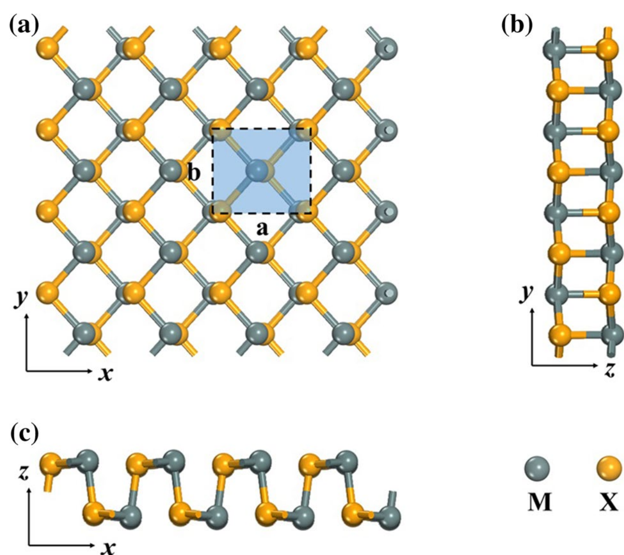

Fig. 1 (a) Top view, (b) side view in the zigzag direction, and (c) side view in the armchair direction of free-standing MXs. The rectangle shows the unit cell (Color figure online).

Table I Lattice parameters, a and b, of fully relaxed ML MXs, structure anisotropy factor κ, defined as $\kappa=(a-b)/(a+b)$, and band gap of ML MXs

	a (Å)	b (Å)	κ	Bandgap (eV)
GeS	4.47	3.67	0.098	1.79 (Indirect)
GeSe	4.26	3.98	0.034	1.14 (Direct)
GeTe	4.38	4.24	0.016	0.89 (Indirect)
SnS	4.44	4.03	0.048	1.61 (Indirect)
SnSe	4.52	4.26	0.030	1.13 (Indirect)
SnTe	4.64	4.56	0.009	0.86 (Indirect)

z-direction, the vacuum space of the periodic model adopts at least 15 Å. The ML MX-metals compound systems are 3×1 Ag(110)/Au(110)–2×1 GeS/GeSe/SnS/SnSe, 1×3 Ag(110)/Au(110)–1×2 GeTe, $5\times\sqrt{3}$ Ag(111)/Au(111)–3×1 SnTe, $2\times\sqrt{3}$ Gr–1×1 GeTe/SnS/SnSe/SnTe, $3\times\sqrt{3}$ Gr–1×2 GeS, and 5×2 Gr–1×3 GeSe supercell, and the number of atoms in these compound systems is 12–72. The lattice constant of the metals is adapted to match that of MXs and mismatch degrees of compound systems are 1.28–5.08% (shown in Table II). In the Vienna *ab initio* simulation package (VASP), the geometry optimization and energy band calculations were simulated by the projector-augmented-wave (PAW) pseudopotential and the plane-wave basis set. We have examined that the optimized structure of MX-metals is almost the same via the code of VASP and Quantum ATK.[17] The k-points mesh is sampled as $9\times9\times1$ and $24\times24\times1$ in the Brillouin integration and the cut-off energies are 400 eV and 500 eV. The DFT-D2 method of Grimme is used in simulating the vdW correction,[35,36] and dipole correction is simulated in the z-direction.[37] The convergence standards of force and energy per atom are less than 0.001 eV/Å and 1×10^{-6} eV.

Figure 2 shows the configuration of the MXs FETs, a kind of two-probe (top-contact) with two interfaces model: one is a vertical interface (V-interface) existing at the edge of metal and MXs, and the other is a lateral interface (L-interface) existing at the edge of the electrodes and channel. The channel region is about 5 nm optimized MXs, and the source/drain regions are MX-metals compound structures. We use the DFT coupled with non-equilibrium Green's function (NEGF) in the Quantum ATK 2019 package to calculate the quantum

Table II Simulated properties of the 2D MX-metal compound systems. $\bar{\varepsilon}$ is the lattice mismatch between the MXs and metals, d_0 the vertical distance from the bottom MXs atom layer to the topmost metal atom layer, d_{min} the minimum distance of atom to atom from MXs to the metals. Δ is the vertical distance from the topmost layer to the bottom atom layer of MXs in contact with metal electrodes. E_b is the binding energy (each MXs atom) needed to remove the MXs layer from the metal electrodes. W_M and W are the work functions of the metal electrode and the MX-metal compound systems. The work functions of MXs are 5.0 (GeS), 4.45 (GeSe), 4.22 (GeTe), 4.70 (SnS), 4.39 (SnSe), 4.12 (SnTe) eV, respectively

Metal	Ag						Au						Graphene					
W_M (eV)	4.26						5.10						4.60					
MX	GeS	GeSe	GeTe	SnS	SnSe	SnTe	GeS	GeSe	GeTe	SnS	SnSe	SnTe	GeS	GeSe	GeTe	SnS	SnSe	SnTe
$\bar{\varepsilon}$(%)	4.47	1.35	1.61	1.28	2.82	4.17	4.48	1.23	1.74	1.28	2.95	4.06	1.85	0.93	3.86	5.08	2.79	4.19
d_0 (Å)	2.29	2.29	2.30	1.94	1.96	2.70	2.23	2.33	2.23	2.35	1.88	1.70	3.49	3.13	3.30	3.28	3.62	3.67
d_{min} (Å)	2.60	2.62	2.90	2.64	2.78	3.06	2.50	2.54	2.82	2.62	2.75	2.75	3.52	3.62	3.81	3.75	3.76	3.82
Δ (Å)	2.78	2.67	2.85	3.13	3.21	3.30	2.85	2.81	2.87	3.10	3.25	3.45	2.57	2.69	3.02	2.90	2.83	3.09
E_b (eV/MX)	1.13	0.20	1.13	1.09	0.93	1.44	1.77	1.31	1.74	1.28	1.55	2.40	0.25	0.26	0.33	0.52	0.74	0.33
W (eV)	4.04	4.05	4.08	3.94	3.91	4.29	4.48	4.38	4.61	4.39	4.49	4.57	4.49	4.49	3.98	3.99	3.93	4.16

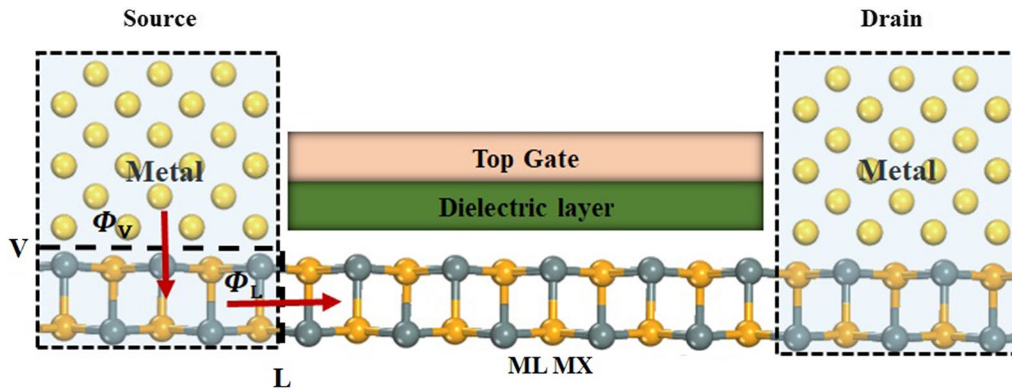

Fig. 2 The structural diagram of MXs FETs. V/L is the vertical/lateral interface where Schottky barriers (Φ_V/Φ_L) may exist. The red arrows denote the pathway of electron or hole carriers from the electrode regions to the channel MXs (Color figure online).

transport of the MXs FETs. The boundary conditions are Neumann (bottom and top of the device) and Dirichlet (on the electrode-channel edges) to ensure electron/hole neutrality. In the irreducible Brillouin zone, the transmission coefficient $T^{kz}(E)$ is the averaged over k_z-points (129) (k_z perpendicular to the transport direction) at the given energy $T(E)$ and is expressed as:

$$T^{kz}(E) = Tr(G^{rkz}(E)\Gamma^{kz}_{L}(E)G^{akz}(E)\Gamma^{kz}_{R}(E)) \quad (1)$$

where $G^{rkz}(E)\left(G^{akz}(E)\right)$ is the retarded (advanced) Green function, respectively. $\Gamma^{kz}_{L/R}(E)$ describe the level broadening zone induced by electrodes and is defined as:

$$\Gamma^{kz}_{L/R}(E) = i\left(\Sigma^{rkz}_{L/R}(E) - \Sigma^{akz}_{L/R}(E)\right) \quad (2)$$

$\Sigma^{kz}_{L/R}(E)$, the electrode self-energies, image the influence of the electrodes on the scattering region.

The pseudopotential type is Hartwigsen-Goedecker-Hutter (HGH) using analytical functions and the hierarchical basis set is Tier3[38] in the Quantum ATK. In the channel (electrodes) region of the device, k-points Monkhorst-Pack meshes take sampling with 19 × 1 × 129 in the irreducible Brillouin zone. The temperature is 300 K, and the exchange-correlation functional is the generalized gradient approximation (GGA) proposed by Perdew-Burke-Ernzerhof (PBE). The single electron theory (DFT-PBE) can be excellent to simulate the electron-electron interactions of 2D transistors because the doping carriers of the electrodes are well screened for the action of the electrons in the channel region. For example, the bandgap of ML $MoSe_2$ by simulation (1.52 eV) (DFT-PBE) is almost the same as experimental (1.58 eV).[39,40] The simulated transport gaps of the ML/bilayer (BL)/trilayer (TL) BP FETs with the Ni electrode are 0.26/0.19/0.20 eV these are in agreement with the value of experimental 0.35/0.23/0.21 eV.[41–44]

Results and Discussion

Models and Electronic Structure Simulation

Three initial structures of high symmetry stacking patterns are considered for relaxation. The most optimized compound systems are shown in Fig. 3 and Supplementary Figures S1-S2. The pucker structure of MXs reserved very well when contacted with the Gr electrode, while Gr has a waved structure in the original plane when it is contacted with GeSe, GeTe, and SnS. The waved structure of Gr contacted with MXs is because of changing the lattice parameter to match the MXs', but symmetrical strain distribution (keeping the hexagonal symmetry structure of Gr unchanged) could not change the electronic properties (conductor characterization) of Gr as the electrode.[45] Most pucker structures of MXs are preserved well when they are contacted with Ag and Au electrodes, as shown in Supplementary Figures S1-S2, while a tiny change on the pucker SnSe when contacted with Ag and Au. The deformed significantly of Au electrode contacted with SnTe be same as Au contacted with stanene, which may be because of considering vdW corrections at the DFT-D3 level with Becke-Jonson damping.[34]

The binding energy E_b of the MX-metals is expressed as:

$$E_b = \left(E_{MX} + E_{metal} - E_{compound}\right)/N_{MX} \quad (3)$$

where E_{MX} is the energy of MXs, E_{metal} is the energy of metal electrode, and $E_{compound}$ is the compound system's

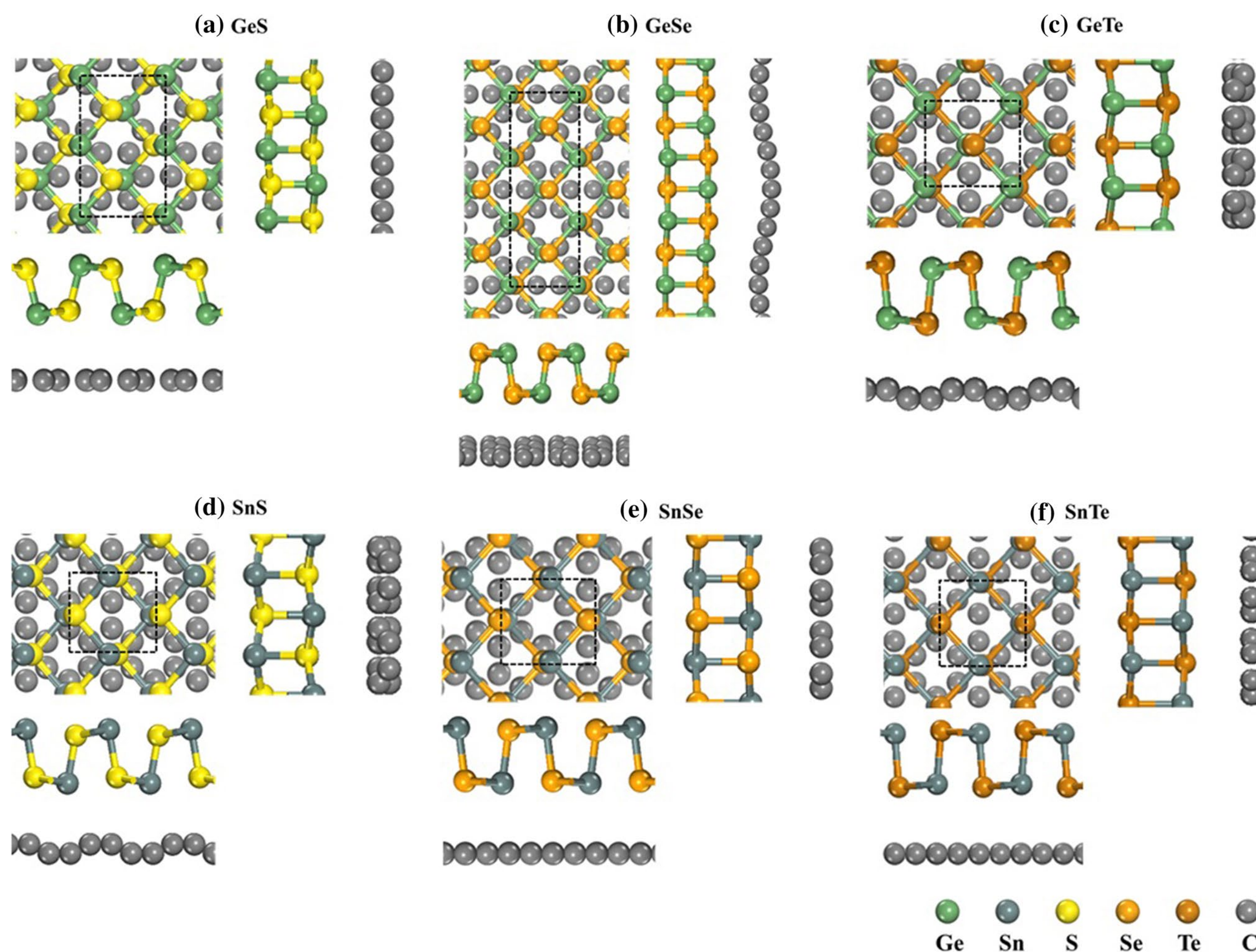

Fig. 3 Top views and side views of the stable configuration for (a) GeS (1×2) on the Gr ($\sqrt{3}$×3), (b) GeSe (1×3) on the Gr (1×5), (c) GeTe (1×1) on the Gr ($\sqrt{5}$×2), (d) SnS (1×1) on the Gr (2×$\sqrt{3}$), (e) SnSe (1×1) on the Gr (2×$\sqrt{3}$), and (f) SnTe (1×1) on the Gr (2×$\sqrt{3}$). The black rectangles represent the unit cells (Color figure online).

energy per supercell, respectively. N_{MX} is the amount of MXs atoms per supercell.

The E_b of MX-Gr compound systems increase in the order of GeS (0.25) = GeSe (0.25) < SnTe (0.32) < GeTe (0.33) < SnS (0.52) < SnSe (0.74 eV), and they are all weaker than those of MX-Ag/Au, except GeSe-Ag (0.20 eV). This weak binding energy of MX-Gr compound systems is due to a weak chemical bonding. From the data (as shown in Table II), weak chemical bonding offered in MX-Gr compound systems with larger interfacial distance, d_0, (3.13–3.67 Å) and larger minimum atom-to-atom distance, d_{min} (3.52–3.82 Å).

The E_b of MX-Ag/Au compound systems increase in the order of GeSe (0.20) < SnSe (0.93) < SnS (1.09) < GeTe (1.13) = GeS (1.13) < SnTe (1.44 eV)/ SnS (1.28) < GeSe (1.31) < SnSe (1.55) < GeTe (1.74) < GeS (1.77) < SnTe (2.40 eV). The interfacial distance of compound systems is in the range of 1.94–2.70 Å/1.70–2.35 Å, and the minimum atom-to-atom distance of compound systems is in the range of 2.60–3.06/2.50–2.82 Å. Compared with Gr and Ag electrode, the E_b of Au electrode is the largest one corresponding to the same MXs, such as $E_{b(GeS\text{-}Gr)} < E_{b(GeS\text{-}Ag)} < E_{b(GeS\text{-}Au)}$, $E_{b(SnS\text{-}Gr)} < E_{b(SnS\text{-}Ag)} < E_{b(SnS\text{-}Au)}$, $E_{b(SnSe\text{-}Gr)} < E_{b(SnSe\text{-}Ag)} < E_{b(SnSe\text{-}Au)}$ and so on, however, interfacial distance and minimum atom-to-atom distance of MX-Au compound systems are not the shortest one.

Figure 4 shows the band structures of the ML MXs. In our calculation, most MXs have indirect band gaps in the range of X–Y, but GeSe has a direct bandgap located in the range of X–Γ. The value and type of GeSe's bandgap depended strongly on the DFT-optimized lattice parameters[46] by theoretical prediction, and the indirect-to-direct band-transformation of GeSe can be obtained by the biaxial strain.[47] The lattice strain could be applied directly, via a substrate, or heterostructure in experimental. The values of bandgap decrease in the order of GeS (1.78) > SnS (1.61) > GeSe

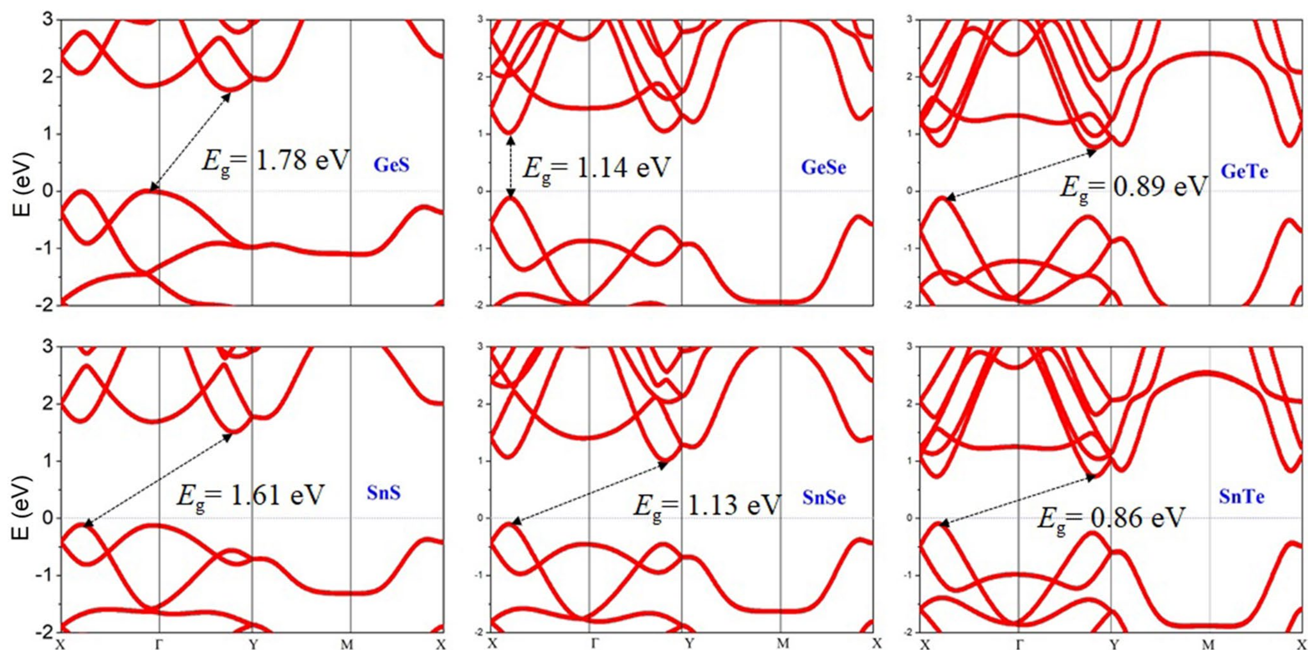

Fig. 4 Band structure of freestanding MXs, respectively (Color figure online).

(1.14) > SnSe (1.13) > GeTe (0.89) > SnTe (0.86 eV). For the same *X*, the bandgap of GeX is larger than that of SnX, because Ge has a smaller atomic number than Sn resulting in a stronger interaction between Ge & *X* atom. Samely the bandgap of MXs decreases in the order of MS>MSe>MTe, since the atomic number of *X* increases in the order of S < Se < Te, resulting in the strength of interaction between *M* & *X* decreases in the order of MS > MSe > MTe.[12,48,49] That is to say the stronger interaction of *M* and *X*, the bigger bandgap of MXs. For the same reason, the structure anisotropy factor κ of ML MXs decrease in the same order GeS (0.098) > SnS (0.048) > GeSe(0.034) > SnSe(0.03) > GeTe (0.016) > SnTe (0.009). This is also because the atomic orbitals are increasing and the interaction of *M* and *X* is becoming stronger. Such behavior is consistent with the bandgap trend of GaX(S, Se, Te) and MX_2(M = Mo, W; X = S, Se, Te), which also decreases from *S* to Te.[50–52]

The band structures of MX-Gr compound systems are shown in Fig. 5, and the red dots and their radii detail the band and the weight of MXs atoms in systems. The ML GeSe-, GeTe-, GeS-, SnSe-, and SnS-Gr compound systems form a *p*-type Schottky contact, and the vertical hole SBH $\left(\Phi^h_{B,V}\right)$ are 0.17 eV, 0.19 eV, 0.36 eV, 0.42 eV, and 0.68 eV, respectively. Interestingly, the SnTe-Gr compound system has a vertical *p*-type Ohmic contact. In the V-interface of MX-Gr, the band gaps are 0.80 (GeTe (0.89)), 0.83 (SnTe(0.86)), 1.11 (SnSe(1.13)), 1.14 (GeSe(1.14)), 1.65 (SnS(1.61)), and 1.66 eV (GeS(1.79 eV)), which are almost in agreement with the bandgap of the ML MXs. The bandgap, band structure, and semiconductor characteristics of ML MXs in the MX-Gr compound systems are almost the same as the freestanding MXs because a weak vdW contact or weak interaction is formed in the V-interface. Gr always be used as a direct contact electrode or as the insertion between the channel and a metal electrode to improve the performance of 2D FETs. Such as GeSe FETs with the Gr electrode and the insertion of the Gr electrode have higher performance than only Cu as the electrode.[17] ML arsenene FETs with Gr electrode has an atomically sharp and ultraclean interface that depressed MIGS and defects in the *V*-interface.[33] ML SnSe on the Gr substrate can be fabricated undamaged through the STM tip controlled because of weak interaction between them, and the size of the ML SnSe plate is about 50 nm.[53] The MXs-Gr heterostructures always have vdW contact type due to weak interaction, this induces a kind of method to manufacture by stacking and transferring techniques of STM or in situ scanning probe manipulations, so fabricating sub-10 nm MXs FETs in the laboratory is likely to be feasible.

Supplementary Figures S3 and S4 show the band structures of MXs in contact with Ag and Au electrodes, respectively. The Fermi level always crosses the energy bands, which means that ML MXs undergo metallization after contact with Ag/Au electrodes for the intense bands hybridized. However, the band hybridization degree of ML SnTe-Ag/Au is the strongest in MX- Ag/Au compound systems, which is in agreement with the binding energy.

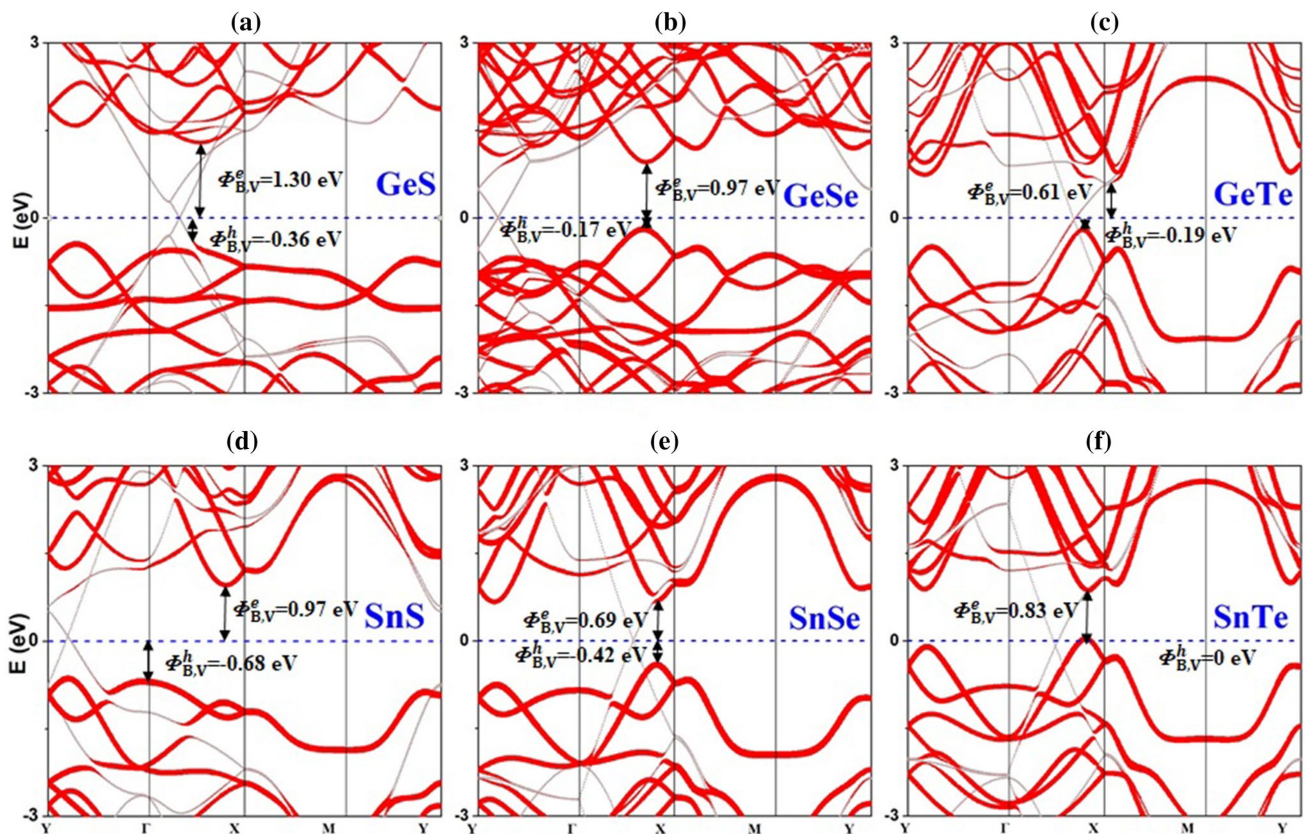

Fig. 5 Energy band graph of the MXs with Gr electrode, respectively. Gray dots correspond to the MX-Gr compound systems. Red dots correspond to the states with valid contributions from MXs, and the radii of the dots are proportional to the weight. (b) reproduced from Ref. 17 © IOP Publishing Ltd. All rights reserved (Color figure online).

This indicates that a strong covalent bond is formed at the V-interface of MX-Ag/Au and ML MXs are chemically adsorbed on Ag/Au electrode. Therefore, an Ohmic contact is formed in the V-interface of MX-Ag/Au compound systems, and the Schottky contact may be in the L-interface.

Quantum Transport Properties and Lateral Interface of the MXs FETs

We assumed the 5 nm MXs FETs with a two-probe model (top-contact) (as shown in Fig. 2). In this kind of two interfaces FETs model, electrons/charges flow from the metal electrode through the V-interface to the L-interface into the 2D MXs channel in general. Therefore, the SBH in V- and L-interface should be analyzed in MXs FETs. The contact of MXs FETs can be classified into vdW contact, weak chemical contact, and strong chemical contact corresponding to weak adhesion, medium adhesion, and strong adhesion.[54] Such as MX-Gr FETs have the vdW or weak chemical contact because the interfacial distance is larger than 3 Å and the band structure of MXs is well preserved without hybridization. Hence, the SBH of electron or hole, Φ^e_L or Φ^h_L, will exist at the V- and L-interface. On the other side, MX-Ag/Au FETs have a strong chemical bonding because the interfacial distance is below 3 Å and the band structure of MXs is strongly hybridized, then the SBH generally disappears at V-interface and will exist at the L-interface.

Figure 6 shows the 5 nm MX-Gr FETs under the zero-bias and zero-gate voltage local density of states (LDOS) projected on the MXs and transmission spectrum of devices. The lateral Schottky barriers ($\Phi^e_{T,L}$ or $\Phi^h_{T,L}$ as shown in white lines with the arrows) of MXs FETs simulated by the QTS defined as

$$\Phi^e_{T,L} = E_{\text{CBM}} - E_f \tag{4}$$

$$\Phi^h_{T,L} = E_f - E_{\text{VBM}} \tag{5}$$

where E_{CBM} and E_{VBM} are the CBM and VBM of the channel MXs at the L-interface. As the bandgap of MXs in the channel, the bands are bending in the LDOS indicating a potential induced by MIGS inserted in the L-interface and leading

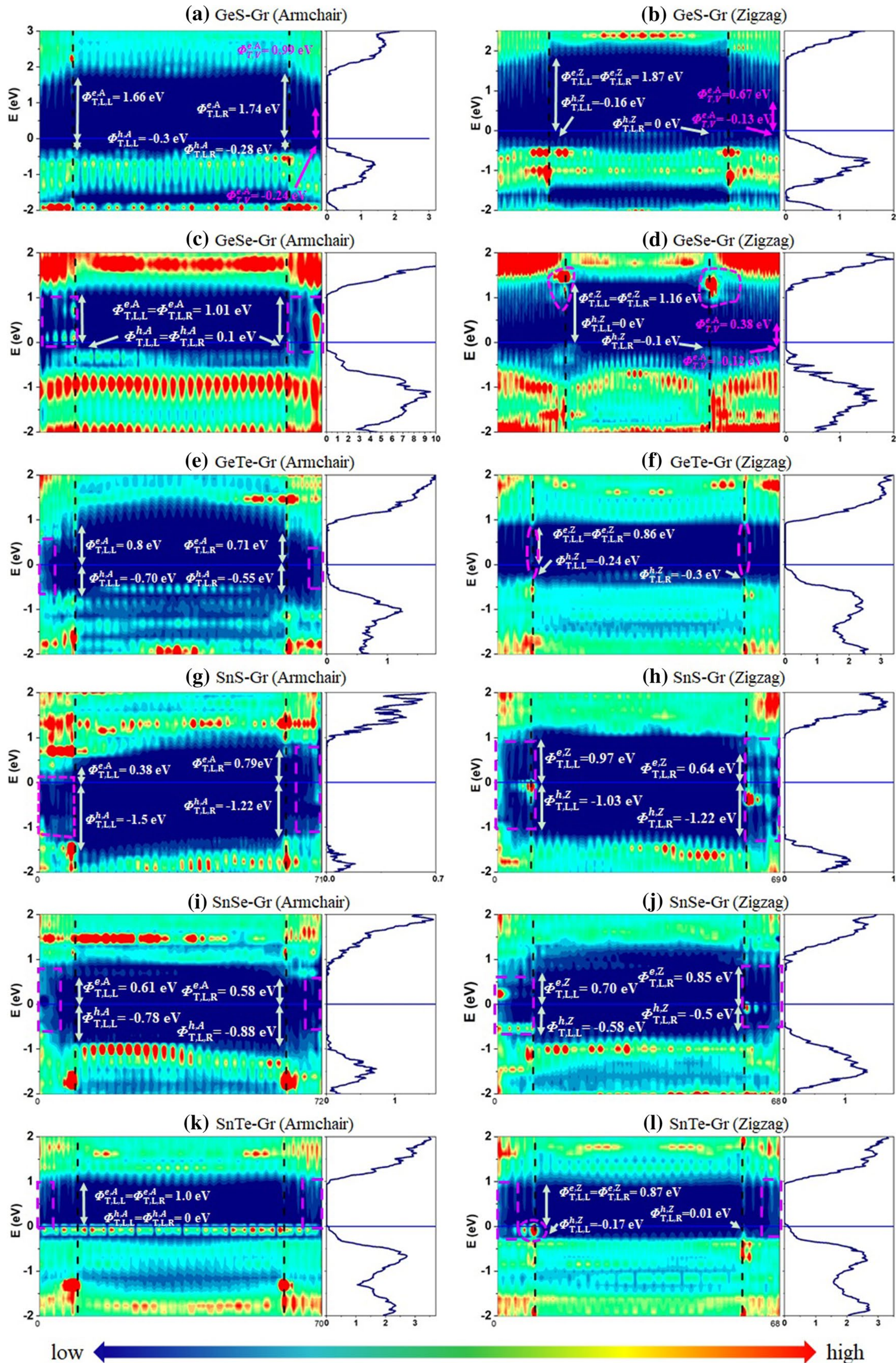
(a) GeS-Gr (Armchair)
(b) GeS-Gr (Zigzag)
(c) GeSe-Gr (Armchair)
(d) GeSe-Gr (Zigzag)
(e) GeTe-Gr (Armchair)
(f) GeTe-Gr (Zigzag)
(g) SnS-Gr (Armchair)
(h) SnS-Gr (Zigzag)
(i) SnSe-Gr (Armchair)
(j) SnSe-Gr (Zigzag)
(k) SnTe-Gr (Armchair)
(l) SnTe-Gr (Zigzag)
E (eV)
low
high

◂**Fig. 6** Local density of states (LDOS) projected on the MXs and Transmission spectrum (TS) of MXs FETs (channel-length~5 nm) with Gr electrode under the zero-bias and zero-gate voltage. The Fermi level is at zero energy. Magenta lines surrounding the area are the region with gap states. (c) and (d) reproduced from Ref. 17 © IOP Publishing Ltd. All rights reserved (Color figure online).

to the difference of the left and right electron (hole) SBH. Therefore, the lateral hole (electron) SBH $\Phi^{e(h)}_{T,L}$ $\left(\Phi^{e(h)}_{T,L} = (\Phi^{e(h)}_{T,L,L} + \Phi^{e(h)}_{T,L,R})/2\right)$, which is the average value between the left and right electron (hole) SBH. In the laboratory by transmission electron microscopy (TEM) and polarization-dependent Raman scattering, the cleavage directions of GeSe nanosheet and layered SnSe are confirmed experimentally, suggesting a pathway to confirm the direction of anisotropic materials.[8,24] Therefore, the direction of ML MXs is feasible to be confirmed in the experiment in this way. Considering the anisotropic MXs, two directions are taken as transport directions of the device: armchair and zigzag direction. Along armchair direction: the GeSe, GeS, and GeTe with Gr electrode form *p*-type lateral Schottky contact, and the hole SBH are 0.1 eV, 0.29 eV, and 0.63 eV, respectively. Intriguingly, a desirable *p*-type Ohmic contact is obtained in SnTe with the Gr electrode. The SnS and SnSe with Gr electrode form *n*-type lateral Schottky contact and the electron SBH are 0.59 eV and 0.6 eV, respectively. Along zigzag direction: The GeTe and SnSe with Gr electrode form *p*-type lateral Schottky contact and the hole SBH are 0.27 eV and 0.54 eV, respectively. The GeSe, GeS, and SnTe FETs have the hole SBH of 0.05 eV, 0.08 eV, and 0.09 eV, respectively, which could be look as quasi *p*-type Ohmic contact for little SBH. The SnS with Gr electrode forms *n*-type lateral Schottky contact of 0.81 eV electron SBH. The SBH valuated by the LDOS is in agreement with that of the transmission spectrum. The Ohmic contact or quasi Ohmic contact suggests the potential of Gr as an excellent electrode of SnTe/GeS/GeSe FETs with high charge injection efficiency, specifically suitable for transistor device applications. 2D FETs with Gr electrode always obtain a vdW contact, which usually weakens or even eliminates the MIGS and Fermi level pinning at the interface. Therefore, use it to avoid or reduce the SBH of devices in the previous work.[9,17,31,55–57]

LDOS offers more details of the V-interface in the deep electrode region, and the bandgap of MXs and type contact are instantly recognizable. In the MX-Gr device, a vdW contact is formed in the electrode region of GeS (armchair and zigzag) and GeSe (zigzag) for lacking or few gap states, as shown in Fig. 6. These results are in agreement with the binding energy of the MX-Gr compound system where GeS- and GeSe-Gr have smaller binding energies. The vertical SBH can be clearly defined by LDOS in the deep electrode region as shown in magenta words and straight lines with arrows. The hole SBH is formed in both armchair and zigzag direction of GeS-Gr FETs, and the values are 0.24/0.13 eV. The contact type is in agreement with the results of band calculations, while the values are smaller band calculations $\left(\Phi_{B,V} = 0.36 \text{ eV}\right)$. That is due to the gap states continuing the CBM and VBM of the electrode region into the gap and reducing the hole SBH. The GeSe has very strong anisotropic interfacial properties,[14,17] therefore, a different contact type in the electrode region is formed in the zigzag (vdW contact) and armchair direction (weak chemical contact). A weak chemical contact is also formed in the electrode region of GeTe (armchair and zigzag), SnS (armchair and zigzag), SnSe (armchair and zigzag), and SnTe (armchair and zigzag) for strong gap states. The gap states herein covered the MIGS and the states of the MXs originating from hybridization with the Gr states, and magenta lines surrounding the area are the region of gap states, therefore, the Φ_V and Φ_L of MX-Gr FETs would be different.

Supplementary Figures S5 and S6 are the LDOS projected on the MXs of MXs FETs with Ag/Au electrodes under the zero-bias and zero-gate voltage and transmission spectrum of devices. A strong chemical contact is formed in the electrode region of MXs FETs, the covalent bonds disturb strongly the band structure of the MXs so that the bandgap of the MXs entirely vanishes in source and drain regions, and carrier injection is barrier-free in the V-interface. The electrode regions of MX-Ag/Au compound systems could be tread as a new metal, which contacts with MXs in the L-interface, therefore, gap states and SBH can only be found in this lateral contact. The MXs FETs with Ag electrodes have the same contact type in both armchair and zigzag directions: *n*-type lateral Schottky contact is formed in the GeS, GeSe, GeTe, and SnS device, and the electron SBH is 0.54/0.56 eV, 0.42/0.29 eV, 0.31/0.12 eV, and 0.78/0.66 eV, respectively. *p*-type lateral Schottky contact is formed in the SnSe and SnTe device, and the hole SBH are 0.58/0.41 and 0.19/- eV, respectively. The MX-Au FETs are all *p*-type lateral Schottky contact along armchair direction, and the hole SBH are 0.24 (GeSe), 0.31(SnTe), 0.32 (GeTe), 0.36 (SnSe), 0.64 (SnS), and 0.8 (GeS) eV. Along the zigzag direction, the GeTe-, SnSe-, SnS-, and GeS-Au FETs have *p*-type lateral Schottky contact with the hole SBH of 0.27 eV, 0.3 eV, 0.57 eV, and 0.58 eV, respectively, and GeSe-Au FETs has *n*-type lateral Schottky with 0.53 eV electron SBH.

There are two methods to get the lateral Schottky barriers (Φ_L): one is the QTS, and the other is a conventional method: work function approximation (WFA). The WFA defines the lateral Schottky barriers ($\Phi^e_{W,L}$ or $\Phi^h_{W,L}$) of MXs FETs as the difference values between the Fermi level of the electrode and CBM/VBM of the channel semiconductor (as shown in Table III). Figure 7 shows the histogram of electron and hole

Table III The transported properties of the ML MXs FETs. $\Phi^{e}_{W,L}$ $\left(\Phi^{h}_{W,L}\right)$ is electron (hole) Schottky barrier heights (SBHs) using the work function approximation. $\Phi^{e,A}_{T,L}$ and $\Phi^{e,Z}_{T,L}$ ($\Phi^{h,A}_{T,L}$ and $\Phi^{h,Z}_{T,L}$) are the electron (hole) SBHs using the transport simulation along armchair and zigzag direction, respectively. $E^{L,A}_{g}$ and $E^{L,Z}_{g}$ are the transport gap along armchair and zigzag direction, respectively

Metal	Graphene						Ag						Au					
MX	GeS	GeSe	GeTe	SnS	SnSe	SnTe	GeS	GeSe	GeTe	SnS	SnSe	SnTe	GeS	GeSe	GeTe	SnS	SnSe	SnTe
$\Phi^{e}_{B,V}$(eV)	1.30	0.97	0.61	0.97	0.69	0.83	0	0	0	0	0	0	0	0	0	0	0	0
$\Phi^{h}_{B,V}$(eV)	0.36	0.17	0.19	0.68	0.42	0	0	0	0	0	0	0	0	0	0	0	0	0
$\Phi^{e}_{W,L}$(eV)	0.39	0.61	0.20	0.10	0.11	0.47	0	0.17	0.30	0.05	0.09	0.60	0.37	0.50	0.83	0.50	0.67	0
$\Phi^{h}_{W,L}$(eV)	1.40	0.53	0.69	1.51	1.02	0.39	0	0.97	0.59	1.56	1.04	0.26	1.42	0.64	0.06	1.11	0.46	0
$\Phi^{e,A}_{T,L}$(eV)	1.70	1.01	0.76	0.59	0.6	1.0	0.54	0.42	0.31	0.78	0.67	0.52	0.89	0.89	0.37	1.01	0.55	0.6
$\Phi^{h,A}_{T,L}$(eV)	0.29	0.1	0.63	1.36	0.8	0	1.25	0.75	0.36	0.85	0.58	0.19	0.8	0.24	0.32	0.64	0.36	0.31
$\Phi^{e,Z}_{T,L}$(eV)	1.87	1.16	0.86	0.81	0.78	0.87	0.56	0.29	0.12	0.66	0.5	–	1.14	0.53	0.4	0.99	0.76	–
$\Phi^{h,Z}_{T,L}$(eV)	0.08	0.05	0.27	1.13	0.54	0.09	1.05	0.78	0.47	0.91	0.41	–	0.58	0.55	0.27	0.57	0.3	–
$E^{T,A}_{g}$(eV)	1.99	1.11	1.39	1.95	1.4	1.0	1.79	1.17	0.67	1.63	1.25	0.71	1.69	1.13	0.69	1.65	0.91	0.91
$E^{T,Z}_{g}$(eV)	1.97	1.21	1.13	1.94	1.32	0.96	1.61	1.07	0.57	1.57	0.91	–	1.72	1.08	0.67	1.56	1.06	–

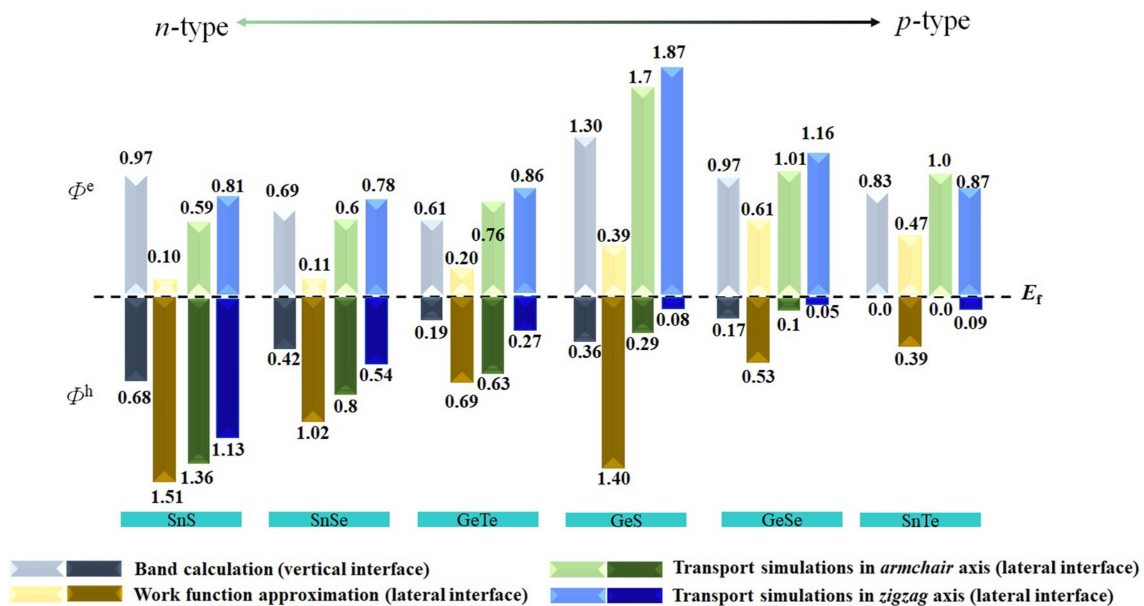

Fig. 7 Electron and hole SBHs of the ML MXs FETs with Gr electrodes from the work function approximation, band calculation, and the transport simulations in the armchair and zigzag direction, respectively.

SBH of the MX-Gr FETs simulating by WFA, band calculation, and QTS. The GeSe-Gr have the same contact type in these three methods. The GeS-, GeTe-, and SnTe-Gr FETs have the same contact (*p*-type) by QTS and band calculation, which is contrary to the result of WFA(*n*-type). SnS-Gr FETs have the same contact (*n*-type) by QTS and WFA, contrary to the band calculation (*p*-type). While the contact type of the SnSe-Gr is *p*-, *n*-, *n* -, and *p*-type by WFA, band calculation, QTS(armchair), and QTS(zigzag).

The band calculation generally is used to determine the SBH in the V-interface and estimate the lateral SBH, and the WFA generally is used to determine the SBH in the L-interface of FETs when a metallization of underlying MXs occurs. These two methods have ignored the coupling between the electrode regions and the MXs channel at L-interface and the gap states at L-interface are also ignored, resulting in inaccuracy. The QTS can accurately define the SBH both in V- and L-interface by LDOS, because LDOS depicts the CBM/VBM edges and gap states clearly in V- and L-interface. Correspondingly, the MIGS and the Fermi level pinning at both interfaces are considered by QTS. Therefore, if the difference between

the SBH obtained from the QTS and band calculation/WFA is observed, the result of QTS is dependable. For example, the pinning factor of the ML MoS_2 reported experimentally is 0.09–0.11, which is well consistent with the QTS of 0.187 rather than 0.27–0.32 (band calculation/WFA).[54]

Conclusions

In conclusion, the interfacial properties of the MX-Gr/Ag/Au compound systems were systematically studied. The MXs preserved semiconductors after being contacted with the Gr electrode and formed weak binding energy, vdW contact, and weak chemical contact type. Along armchair direction, the GeSe- (0.1), GeS- (0.29), and GeTe- (0.63 eV)Gr FETs form *p*-type lateral Schottky contact, and the SnS- (0.59) and SnSe- (0.6 eV)Gr FETs form *n*-type lateral Schottky contact, respectively. Along zigzag direction, the GeSe- (0.05), GeS- (0.08), SnTe- (0.09), GeTe- (0.27) and SnSe- (0.54 eV) Gr FETs form *p*-type lateral Schottky contact, and the SnS-Gr (0.81 eV) FETs forms *n*-type lateral Schottky contact. In the V-interface, the MXs undergo a metallization after being contacted with Ag and Au electrodes and form strong binding energy. In the L-interface, the MX- Ag/Au FETs have a lateral Schottky contact. The GeS (0.54/0.56), GeSe (0.42/0.29), GeTe (0.31/0.12), and SnS (0.78/0.66 eV) with Ag electrodes have *n*-type lateral Schottky contact, and the SnSe (0.58/0.41) and SnTe (0.19/- eV) device have *p*-type lateral Schottky contact in the armchair/zigzag direction. The MX- Au FETs have a *p*-type lateral Schottky contact with the hole SBH of 0.24 (GeSe), 0.31(SnTe), 0.32 (GeTe), 0.36 (SnSe), 0.64 (SnS), and 0.8 (GeS) eV along armchair direction, respectively. The GeTe- (0.27), SnSe- (0.3), SnS- (0.57), and GeS- (0.58 eV)Au device along zigzag direction have *p*-type lateral Schottky contact, respectively, and the GeSe-Au (0.53 eV) device along zigzag direction has *n*-type lateral Schottky contact. A desired *p*-type Ohmic contact is formed in the SnTe (armchair), and quasi *p*-type Ohmic contact is formed in the GeS (zigzag), GeSe (zigzag), and SnTe (zigzag) FETs with the Gr electrode due to little SBH. Our investigation reveals the potential of contact properties in MXs FETs device applications.

Supporting Information Available

Stable configuration of MXs contacted with Ag and Au electrodes. Energy band graph of MXs with Ag and Au electrodes; LDOS in color-coding projected on ML MXs and TS of the MXs FETs with Ag and Au electrodes.

Supplementary Information The online version contains supplementary material available at https://doi.org/10.1007/s11664-022-09747-9.

Acknowledgment The National Natural Science Foundation of China (Nos. 11704406/11674005), the Natural Science Basic Research Program of Shaanxi, China (Program No. 2022JM-046/2022JM-051), and the Natural Science Foundation of Shaanxi Provincial Department of Science and Technology (Program No. 2021IQ-749) support this work.

Conflict of interest The authors declare that they have no conflict of interest. This research received no funding.

References

1. R. Quhe, L. Xu, S. Liu, C. Yang, Y. Wang, H. Li, J. Yang, Q. Li, B. Shi, Y. Li, Y. Pan, X. Sun, J. Li, M. Weng, H. Zhang, Y. Guo, L. Xu, H. Tang, J. Dong, J. Yang, Z. Zhang, M. Lei, F. Pan, and J. Lu, *Phys. Rep.* 938, 1 (2021).
2. L. Li, Y. Yu, G.J. Ye, Q. Ge, X. Ou, H. Wu, D. Feng, X.H. Chen, and Y. Zhang, *Nat. Nanotechnol.* 9, 372 (2014).
3. Z. Yu, Z.Y. Ong, Y. Pan, Y. Cui, R. Xin, Y. Shi, B. Wang, Y. Wu, T. Chen, Y.W. Zhang, G. Zhang, and X. Wang, *Adv. Mater.* 28, 547 (2016).
4. I.S.S. de Oliveira and R. Longuinhos, *Phys. Rev. B* 94, 035440 (2016).
5. L. Xu, M. Yang, S.J. Wang, and Y.P. Feng, *Phys. Rev. B* 95, 235434 (2017).
6. P.Z. Hanakata, A. Carvalho, D.K. Campbell, and H.S. Park, *Phys. Rev. B* 94, 035304 (2016).
7. G. Shi and E. Kioupakis, *Nano Lett.* 15, 6926 (2015).
8. S. Yang, Y. Liu, M. Wu, L.-D. Zhao, Z. Lin, H.-C. Cheng, Y. Wang, C. Jiang, S.-H. Wei, L. Huang, Y. Huang, and X. Duan, *Nano Res.* 11, 554 (2017).
9. R. Quhe, X. Peng, Y. Pan, M. Ye, Y. Wang, H. Zhang, S. Feng, Q. Zhang, J. Shi, J. Yang, D. Yu, M. Lei, J. Lu, and A.C.S. Appl, *Mater. Interfaces* 9, 3959 (2017).
10. J. Yan, H. Pang, L. Xu, J. Yang, R. Quhe, X. Zhang, Y. Pan, B. Shi, S. Liu, L. Xu, J. Yang, F. Pan, Z. Zhang, and J. Lu, *Adv. Electron. Mater.* 5, 1900226 (2019).
11. Y. Guo, S. Zhou, Y. Bai, and J. Zhao, *ACS Appl. Mater. Interfaces* 9, 12013 (2017).
12. E. Sutter, J.S. French, and P. Sutter, *Nanoscale* 14, 6195 (2022).
13. Y. Ding, Y.-S. Liu, G. Yang, Y. Gu, Q. Fan, N. Lu, H. Zhao, Y. Yu, X. Zhang, X. Huo, and G. Chen, *ACS Appl. Electron. Mater.* 3, 1151 (2021).
14. Y. Guo, F. Pan, G. Zhao, Y. Ren, B. Yao, H. Li, and J. Lu, *Nanoscale* 12, 15443 (2020).
15. H. Li, P. Xu, and J. Lu, *Nanoscale* 11, 23392 (2019).
16. P.C. Shen, C. Su, Y. Lin, A.S. Chou, C.C. Cheng, J.H. Park, M.H. Chiu, A.Y. Lu, H.L. Tang, M.M. Tavakoli, G. Pitner, X. Ji, Z. Cai, N. Mao, J. Wang, V. Tung, J. Li, J. Bokor, A. Zettl, C.I. Wu, T. Palacios, L.J. Li, and J. Kong, *Nature* 593, 211 (2021).
17. Y. Guo, F. Pan, Y. Ren, Y. Wang, B. Yao, G. Zhao, and J. Lu, *Semicond. Sci. Technol.* 34, 095021 (2019).
18. S. Li, W. Xiao, Y. Pan, J. Jie, C. Xin, J. Zheng, J. Lu, and F. Pan, *J. Phys. Chem. C* 122, 12322 (2018).
19. Y. Ji, M. Yang, H. Dong, L. Wang, T. Hou, and Y. Li, *J. Mater. Chem. A* 5, 1734 (2017).
20. A.K. Singh and R.G. Hennig, *Appl. Phys. Lett.* 105, 042103 (2014).
21. R. Fei, W. Li, J. Li, and L. Yang, *Appl. Phys. Lett.* 107, 173104 (2015).

22. H. Zhao, Y. Mao, X. Mao, X. Shi, C. Xu, C. Wang, S. Zhang, and D. Zhou, *Adv. Funct. Mater.* 28, 1704855 (2018).
23. D.J. Xue, J. Tan, J.S. Hu, W. Hu, Y.G. Guo, and L.J. Wan, *Adv. Mater.* 24, 4528 (2012).
24. X. Zhou, X. Hu, B. Jin, J. Yu, K. Liu, H. Li, and T. Zhai, *Adv. Sci. (Weinh)* 5, 1800478 (2018).
25. B. Mukherjee, Y. Cai, H.R. Tan, Y.P. Feng, E.S. Tok, C.H. Sow, and A.C.S. Appl, *Mater. Interfaces* 5, 9594 (2013).
26. S.M. Yoon, H.J. Song, and H.C. Choi, *Adv. Mater.* 22, 2164 (2010).
27. L. Li, W. Wang, P. Gong, X. Zhu, B. Deng, X. Shi, G. Gao, H. Li, and T. Zhai, *Adv. Mater.* 30, 1706771 (2018).
28. L. Xie, M. Liao, S. Wang, H. Yu, L. Du, J. Tang, J. Zhao, J. Zhang, P. Chen, X. Lu, G. Wang, G. Xie, R. Yang, D. Shi, and G. Zhang, *Adv. Mater.* 29, 1702522 (2017).
29. Y. Liu, H. Wu, H.C. Cheng, S. Yang, E. Zhu, Q. He, M. Ding, D. Li, J. Guo, N.O. Weiss, Y. Huang, and X. Duan, *Nano Lett.* 15, 3030 (2015).
30. O. Lopez-Sanchez, D. Lembke, M. Kayci, A. Radenovic, and A. Kis, *Nat. Nanotechnol.* 8, 497 (2013).
31. Y. Guo, F. Pan, M. Ye, X. Sun, Y. Wang, J. Li, X. Zhang, H. Zhang, Y. Pan, Z. Song, J. Yang, J. Lu, and A.C.S. Appl, *Mater. Interfaces* 9, 23128 (2017).
32. J. Yan, X. Zhang, Y. Pan, J. Li, B. Shi, S. Liu, J. Yang, Z. Song, H. Zhang, M. Ye, R. Quhe, Y. Wang, J. Yang, F. Pan, and J. Lu, *J. Mater. Chem. C* 6, 6153 (2018).
33. Y. Wang, M. Ye, M. Weng, J. Li, X. Zhang, H. Zhang, Y. Guo, Y. Pan, L. Xiao, J. Liu, F. Pan, J. Lu, and A.C.S. Appl, *Mater. Interfaces* 9, 29273 (2017).
34. Y. Guo, F. Pan, M. Ye, Y. Wang, Y. Pan, X. Zhang, J. Li, H. Zhang, and J. Lu, *2D Mater* 3, 035020 (2016).
35. S. Grimme, J. Antony, S. Ehrlich, and H. Krieg, *J. Chem. Phys.* 132, 154104 (2010).
36. S. Grimme, S. Ehrlich, and L. Goerigk, *J. Comput. Chem.* 32, 1456 (2011).
37. J. Neugebauer and M. Scheffler, *Phys. Rev. B* 46, 16067 (1992).
38. K.F. Garrity, J.W. Bennett, K.M. Rabe, and D. Vanderbilt, *Comput. Mater. Sci.* 81, 446 (2014).
39. Y. Liang and L. Yang, *Phys. Rev. Lett.* 114, 063001 (2015).
40. M.M. Ugeda, A.J. Bradley, S.F. Shi, F.H. da Jornada, Y. Zhang, D.Y. Qiu, W. Ruan, S.K. Mo, Z. Hussain, Z.X. Shen, F. Wang, S.G. Louie, and M.F. Crommie, *Nat. Mater.* 13, 1091 (2014).
41. S. Das, W. Zhang, M. Demarteau, A. Hoffmann, M. Dubey, and A. Roelofs, *Nano Lett.* 14, 5733 (2014).
42. Y. Pan, Y. Wang, M. Ye, R. Quhe, H. Zhong, Z. Song, X. Peng, D. Yu, J. Yang, J. Shi, and J. Lu, *Chem. Mater.* 28, 2100 (2016).
43. Y. Pan, Y. Dan, Y. Wang, M. Ye, H. Zhang, R. Quhe, X. Zhang, J. Li, W. Guo, L. Yang, and J. Lu, *ACS Appl. Mater. Interfaces* 9, 12694 (2017).
44. X. Zhang, Y. Pan, M. Ye, R. Quhe, Y. Wang, Y. Guo, H. Zhang, Y. Dan, Z. Song, J. Li, J. Yang, W. Guo, and J. Lu, *Nano Res.* 11, 707 (2017).
45. G. Gui, J. Li, and J. Zhong, *Phys. Rev. B* 78, 075435 (2008).
46. H. Shin, J.T. Krogel, K. Gasperich, P.R.C. Kent, A. Benali, and O. Heinonen, *Phys. Rev. Mater.* 5, 024002 (2021).
47. Y. Hu, S. Zhang, S. Sun, M. Xie, B. Cai, and H. Zeng, *Appl. Phys. Lett.* 107, 122107 (2015).
48. L. Huang, F. Wu, and J. Li, *J. Chem. Phys.* 144, 114708 (2016).
49. Y. Wang, C. Qiu, C. Shen, L. Li, K. Yang, Z. Wei, H.X. Deng, and C. Xia, *J. Phys. Condens. Matter.* 34, 195003 (2022).
50. S. Bhattacharyya and A.K. Singh, *Phys. Rev. B* 86, 075454 (2012).
51. L. Huang, Z. Chen, and J. Li, *RSC Adv.* 5, 5788 (2015).
52. J. Kang, S. Tongay, J. Zhou, J. Li, and J. Wu, *Appl. Phys. Lett.* 102, 012111 (2013).
53. K. Chang, F. Kuster, B.J. Miller, J.R. Ji, J.L. Zhang, P. Sessi, S. Barraza-Lopez, and S.S.P. Parkin, *Nano Lett.* 20, 6590 (2020).
54. Y. Wang, S. Liu, Q. Li, R. Quhe, C. Yang, Y. Guo, X. Zhang, Y. Pan, J. Li, H. Zhang, L. Xu, B. Shi, H. Tang, Y. Li, J. Yang, Z. Zhang, L. Xiao, F. Pan, and J. Lu, *Rep. Prog. Phys.* 84, 056501 (2021).
55. Y. Liu, N.O. Weiss, X. Duan, H.-C. Cheng, Y. Huang, and X. Duan, *Nat. Rev. Mater.* 1, 16042 (2016).
56. Y. Liu, P. Stradins, and S.H. Wei, *Sci. Adv.* 2, e1600069 (2016).
57. H. Zhang, J. Xiong, M. Ye, J. Li, X. Zhang, R. Quhe, Z. Song, J. Yang, Q. Zhang, B. Shi, J. Yan, W. Guo, J. Robertson, Y. Wang, F. Pan, and J. Lu, *Phys. Rev. Appl.* 11, 064001 (2019).

Publisher's Note Springer Nature remains neutral with regard to jurisdictional claims in published maps and institutional affiliations.